Survival of the Quantum Anomalous Hall Effect in Orbital Magnetic Fields as a Consequence of the Parity Anomaly

Jan Böttcher[†] and Christian Tutschku[†]
Institut für theoretische Physik (TP4) and Würzburg-Dresden Cluster of Excellence ct.qmat, Universität Würzburg, 97074 Würzburg, Germany

Laurens W. Molenkamp
Physikalisches Institut (EP3), Universität Würzburg, Am Hubland, 97074 Würzburg, Germany

E. M. Hankiewicz[*]
Institut für theoretische Physik (TP4) and Würzburg-Dresden Cluster of Excellence ct.qmat, Universität Würzburg, 97074 Würzburg, Germany

(Received 18 January 2019; published 26 November 2019)

Recent experimental progress in condensed matter physics enables the observation of signatures of the parity anomaly in two-dimensional Dirac-like materials. Using effective field theories and analyzing band structures in external out-of-plane magnetic fields (orbital fields), we show that topological properties of quantum anomalous Hall (QAH) insulators are related to the parity anomaly. We demonstrate that the QAH phase survives in orbital fields, violates the Onsager relation, and can be therefore distinguished from a quantum Hall (QH) phase. As a fingerprint of the QAH phase in increasing orbital fields, we predict a transition from a quantized Hall plateau with $\sigma_{xy} = -e^2/h$ to a not perfectly quantized plateau, caused by scattering processes between counterpropagating QH and QAH edge states. This transition can be especially important in paramagnetic QAH insulators, such as (Hg, Mn)Te/CdTe quantum wells, in which exchange interaction and orbital fields compete.

DOI: 10.1103/PhysRevLett.123.226602

Introduction.—Condensed matter analogs of the Dirac equation have opened new directions to study quantum anomalies in the solid-state laboratory [1–8]. An anomaly occurs, when a symmetry of a classical theory cannot be maintained in the associated quantum theory [9–11]. For instance, in massless, $(2+1)$D quantum electrodynamics, parity symmetry is broken during regularization if one insists on gauge invariance (parity anomaly) [12–19]. As a consequence, a Chern-Simons (CS) term is induced even in the absence of a magnetic field [3,16].

In condensed matter physics, an analogous system is a Chern (QAH) insulator which describes a single Dirac fermion with a momentum dependent mass or, equivalently, half of the Bernevig-Hughes-Zhang (BHZ) model [20,21]. In our work, we examine hallmarks of the parity anomaly in two-dimensional quantum anomalous Hall (QAH) insulators subjected to an external out-of-plane magnetic field (orbital field). In particular, we demonstrate that the parity anomaly enables us to distinguish the QAH from a quantum Hall (QH) phase. This is due to the fact, that although both phases are described by the same topological invariant, the Chern number [22], their physical origin is very different: QH phases are induced by an orbital field, whereas the QAH phase results from an inverted band structure [23]. Here, inverted means that the ordinary conduction band is below the ordinary valence band. A QAH insulator is characterized by a quantized Hall conductivity $\sigma_{xy} = \mathcal{C}e^2/h$ with $\mathcal{C} = [\mathrm{sgn}(M) + \mathrm{sgn}(B)]/2$ [24], where $2M$ is the bulk band gap (Dirac mass gap) and B is related to the effective mass. In our work, we reveal that this characteristic quantity persists in orbital fields H with

$$\mathcal{C}(H) = [\mathrm{sgn}(M - B/l_H^2) + \mathrm{sgn}(B)]/2, \tag{1}$$

where $l_H = \sqrt{\hbar/|eH|}$. Equation (1) shows that H counteracts the intrinsic band inversion until it eventually overcomes the Dirac mass gap at $M = B/l_{H_{\mathrm{crit}}}^2$. Moreover, it illustrates a violation of the Onsager relation which would require that $\sigma_{xy}(-H) = -\sigma_{xy}(H)$. This is a hallmark of the parity anomaly in magnetic fields. In contrast, a conventional QH phase fulfills the Onsager relation as $\sigma_{xy} \propto \mathrm{sgn}(eH)$.

As a signature of the parity anomaly, the survival of the QAH phase induces a unique type of charge pumping. Increasing the orbital field generates a charge flow from the edges (charge depletion) into the bulk (charge accumulation), starting at $H \neq 0$. Moreover, as a function of H, the QAH edge states are pushed into the bulk valence band, leading to the coexistence of counterpropagating QH and QAH edge states. If disorder is present, these states are not

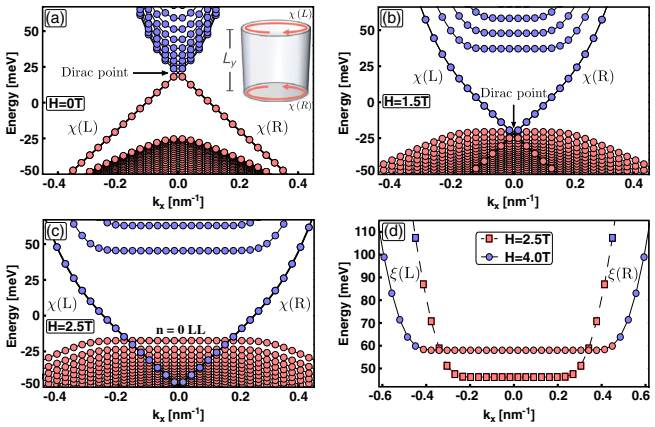

FIG. 1. Band structure of a QAH insulator in orbital fields H (black lines) for $M = -25$ meV, $B = -1075$ meV nm^2, $D = -900$ meV nm^2, and $A = 365$ meV nm. $\chi(L/R)$ and $\xi(L/R)$ depict QAH and QH edge states at the left and right boundary. (a) Spectrum for $H = 0$ at half filling with chiral QAH edge states traversing the bulk gap. The inset depicts the sample geometry. (a)–(c) Evolution of the spectrum and its filling with increasing H, where empty (filled) states are marked in blue (red). (d) Analogous analysis for an initially filled conduction band LL.

protected from backscattering. We predict, that these two effects give rise to a system size dependent transition from $\sigma_{xy} = -e^2/h$ to a not perfectly quantized Hall plateau. The average value of this plateau depends on details of the scattering mechanisms. Such a transition should be observable in (Hg,Mn)Te quantum wells [25] or in Bi-based QAH insulators [26–29].

Model.—We start with a Chern (QAH) insulator described by a single, nontrivial block of the BHZ model:

$$\mathcal{H}(\mathbf{k}) = (M - Bk^2)\sigma_z - Dk^2\sigma_0 + A(k_x\sigma_x - k_y\sigma_y), \tag{2}$$

where $k^2 = k_x^2 + k_y^2$, σ_i are the Pauli matrices, A mixes both (pseudo)spin-components, D introduces a particle-hole asymmetry, and B, as well as M were defined before [20]. The spectrum is obtained numerically by mapping the Hamiltonian on a stripe geometry with finite length L_y in the $\mathbf{e}_y$ direction (hard wall boundary conditions) and periodic boundary conditions along the $\mathbf{e}_x$ direction [30]. In Fig. 1(a), the band structure with $\mathcal{C} = -1$ is displayed, with chiral QAH edge states traversing the Dirac mass gap. Since $D \neq 0$, the Dirac point lies close to the conduction band edge [31].

Next, we implement an orbital field $\mathbf{H} = H\mathbf{e}_z$ in the Landau gauge $\mathbf{A} = -yH\mathbf{e}_x$ [Figs. 1(b) and 1(c)]. This has two main effects: First, bulk subbands evolve into Landau levels (LLs) for $l_H \ll L_y$. All LLs with $n \neq 0$ come in pairs of energy $E_n^{\pm}$, except for the single $n = 0$ LL with energy E_0 [32]. This causes an asymmetry in the spectrum further discussed in Ref. [33]. Second, the orbital field gradually lowers the energy of the Dirac point so that it enters the valence band at $H = H_{\text{scat}}$. The evolution of the Dirac point is determined by $E_D(H) \approx E_D(0) - g_{\text{eff}}\mu_B H$, where $g_{\text{eff}} = m_0 v_x L_y/\hbar$ [31]. Here, v_x is the edge state velocity, μ_B is the Bohr magneton, m_0 is the electron mass, and $E_D(0)$ is the Dirac point energy at $H = 0$. Note that the QAH edge states survive (up to finite size gaps) even for large H [Fig. 1(c)] since they are protected from hybridization with bulk states by their wave function localization.

Effective action.—To understand the survival of the QAH edge states, we derive the corresponding low energy effective bulk Lagrangian $\mathcal{L}_{\text{eff}}^{\text{bulk}}$ by computing the particle number in the continuum or bulk model [15,33],

$$\langle N\rangle_\mu = \frac{1}{2}\int d\mathbf{x}\sum_\alpha \langle[\psi_\alpha^\dagger(\mathbf{x}), \psi_\alpha(\mathbf{x})]\rangle_\mu = \langle N_0\rangle_\mu - \frac{\eta_H}{2}.$$

Here, $\langle\cdots\rangle_\mu$ denotes the expectation value with respect to the chemical potential μ, $\psi(\mathbf{x})$ is a field operator, and N_0 is the fermion number operator, counting the number of filled or empty states with respect to the charge neutrality point. The last term is the spectral asymmetry η_H [15], quantifying the difference in the number of positive and negative eigenvalues of our system. From Lorentz covariance, one can then determine the induced three current $j_{\text{ind}}^\mu = \sigma_{xy}\epsilon^{\mu\nu\rho}\partial_\nu a_\rho$ arising as a response to a small perturbing field a_μ, applied on top of the underlying orbital field H. Here, j_{ind}^0 is the induced bulk charge density, and $j_{\text{ind}}^{1,2}$ is the induced bulk current density in the x and y direction, respectively. Since $j_{\text{ind}}^\mu = \delta S_{\text{eff}}^{\text{bulk}}/\delta a_\mu$ with $S_{\text{eff}}^{\text{bulk}} = \int d^3x \mathcal{L}_{\text{eff}}^{\text{bulk}}$, we can compute the corresponding effective bulk Lagrangian which is one of the main results of our Letter (further details are given in Ref. [33]):

$$\mathcal{L}_{\text{eff}}^{\text{bulk}}(\mu, H) = \frac{\sigma_{xy}(\mu, H)}{2}\epsilon^{\mu\nu\rho}a_\mu\partial_\nu a_\rho, \tag{3}$$

where $\epsilon^{\mu\nu\rho}$ is the Levi-Civita symbol. This is a topological CS term [34] with quantized Hall conductivity

$$\sigma_{xy} = \frac{e^2}{2h}\kappa_{\text{QAH}} - \frac{e^2}{2h}\kappa_{\text{QH}}^0\Theta(|\mu + D/l_H^2| - |M - B/l_H^2|) - \frac{e^2}{h}\sum_{s=\pm,\,n=1}^{\infty} s\kappa_{\text{QH}}\Theta[s(\mu - E_n^s)]. \tag{4}$$

According to their physical origin, we separated σ_{xy} into

$$\kappa_{\text{QAH}} = \text{sgn}(M - B/l_H^2) + \text{sgn}(B), \tag{4a}$$

$$\kappa_{\text{QH}}^0 = \text{sgn}(eH)\text{sgn}(\mu + D/l_H^2) + \text{sgn}(M - B/l_H^2), \tag{4b}$$

$$\kappa_{\text{QH}} = \text{sgn}(eH). \tag{4c}$$

CS terms arise if parity and time-reversal symmetry are broken [16,34]. In our case, they are therefore induced by the mass terms M and Bk^2, as well as by the orbital

field H [33,35]. We distinguish two types of CS terms: The first type, Eq. (4a), is defined by its exclusive relation to M and Bk^2, resulting in the violation of the Onsager relation. This term is a consequence of the parity anomaly at $H = 0$, which requires that a single, parity invariant Chern insulator cannot exist in $(2+1)$D [16]. Its special origin is reflected by the fact that Eq. (4a) is solely determined by the spectral asymmetry $\eta_H = 2n_0 \mathrm{sgn}(eH)\kappa_{\mathrm{QAH}}$, where n_0 is the LL degeneracy. It is a property of the entire eigenvalue spectrum and, hence, does not come along with a Heaviside function. The second type of CS terms, Eqs. (4b) and (4c), describes conventional QH physics, generated by an orbital field, as indicated by their $\mathrm{sgn}(eH)$ dependence. In contrast to the first type, each of these CS terms is related to a single LL, reflected by the Heaviside functions. They can only contribute to the Hall conductivity if $|\mu + D/l_H^2| > |M - B/l_H^2|$.

In order to derive the corresponding edge theories, we have to add a new degree of freedom to $\mathcal{L}_{\mathrm{eff}}^{\mathrm{bulk}}$. This can be inferred from the fact that any CS term changes by a total derivative under a local gauge transformation, $\mathcal{L}_{\mathrm{eff}}^{\mathrm{bulk}} \to \mathcal{L}_{\mathrm{eff}}^{\mathrm{bulk}} + \delta\mathcal{L}_{\mathrm{eff}}^{\mathrm{bulk}}$, causing a violation of charge conservation, $\partial_\mu j^\mu_{\mathrm{ind}} \neq 0|_{\partial\Omega}$, at the boundary $\partial\Omega$ [34,36]. To cancel this U(1) anomaly, we must enlarge our description by an effective edge Lagrangian $\mathcal{L}_{\mathrm{eff}}^{\partial\Omega}$, which restores gauge invariance via anomaly cancellation between the edge and bulk (Callan-Harvey mechanism) [36–39]:

$$\begin{aligned} \partial_\mu j^\mu_{\mathrm{tot}} &= \partial_\mu (j^\mu_{\mathrm{ind}} + j^\mu_L + j^\mu_R) = 0 \\ \Rightarrow \partial_\mu j^\mu_{L/R} &= \frac{\sigma_{xy}}{2}\delta(y - y_{L/R})\epsilon^{2\nu\lambda}\partial_\nu a_\lambda = -\partial_\mu j^\mu_{\mathrm{ind}}, \end{aligned} \tag{5}$$

where $j^\mu_{L/R}$ symbolizes induced currents at the left or right edge of the stripe geometry. This procedure is the field-theoretical analog to the bulk-boundary correspondence [40]. Equation (5) implies that an orbital field induces charge accumulation in the bulk which is compensated by a charge depletion at the edges (fixed total charge) [17,41,42]. The amount of induced bulk charge is given by $j^0_{\mathrm{ind}} = \sigma_{xy}\nabla \times \mathbf{a}$. From Eq. (5), one can deduce

$$\mathcal{L}_{\mathrm{eff}}^{\partial\Omega} = \mathcal{L}_{\mathrm{eff}}^{L}\delta(y - y_L) + \mathcal{L}_{\mathrm{eff}}^{R}\delta(y - y_R),$$

$$\mathcal{L}_{\mathrm{eff}}^{L/R} = \chi^\dagger i\left(\partial_t \mp \frac{h}{e^2}\kappa_{\mathrm{QAH}} D_x\right)\chi \tag{6a}$$

$$+ \xi_0^\dagger i\left(\partial_t \mp \frac{h}{e^2}\kappa_{\mathrm{QH}}^{n=0} D_x\right) \times \xi_0 \Theta(|\mu + D/l_H^2| - |M - B/l_H^2|) \tag{6b}$$

$$+ \sum_{\substack{n=1 \\ s=\pm}}^{\infty} s\xi_n^\dagger i\left(\partial_t \mp \frac{h}{e^2}\kappa_{\mathrm{QH}}^{n} D_x\right)\xi_n \Theta[s(\mu - E_n^s)], \tag{6c}$$

where $\chi(\xi_n)$ defines QAH (QH) edge states and $D_x \equiv \partial_x + iea_\mu/\hbar$. Equation (6a) is linked to Eq. (4a) and characterizes QAH edge states, persisting in orbital fields. The QAH edge states are not bound to a specific LL (no Heaviside function) but instead bridge the gap between valence and conduction band. This finding is in accordance with our band structure calculations, shown in Fig. 1. Since Eq. (6a) is connected to the spectral asymmetry η_H, charge pumping via anomaly cancellation can occur from the QAH edge states into any LL. This pumping mechanism is therefore a signature of the parity anomaly and can, in general, exist until the Dirac mass gap is eventually closed at the critical field [Eq. (4a)]

$$H_{\mathrm{crit}} = \mathrm{sgn}(eH)\frac{\hbar}{e}\frac{M}{B}. \tag{7}$$

In contrast, Eqs. (6b) and (6c) are related to Eqs. (4b) and (4c) and define QH edge states. These states are bound by single LLs and charge flow appears only between edge states and their associated LL.

Charge pumping.—To highlight the differences in the charge pumping between QAH and QH phases, we consider here an impurity-free system and comment on (in)elastic scattering effects in the next section. We simulate the evolution of the charge distribution as a function of the orbital field by solving the time-dependent Schrödinger equation. As in typical experiments, we keep the total charge (not chemical potential) constant in our simulations [25,43–45]. In particular, we consider a vector potential $\mathbf{A}(t) = \mathbf{A}(t_i) + \mathbf{a}(t)$ with $t \in [t_i = 0, t_f]$, where $\mathbf{A}(t_i)$ is a time-independent background field and $\mathbf{a}(t) = -yH(t)\mathbf{e}_x$ is a time-dependent perturbation. At initial time t_i, the system is described by the solutions of the Schrödinger equation $|\psi_{j,k_x}(t_i)\rangle$, where j labels the jth subband. For $t > t_i$, the perturbation is switched on and each initially occupied state, with $j \leq j_{\max}$ and $k \leq k_{\max}$, evolves under unitary time evolution to $|\psi_{j,k_x}(t)\rangle$ [46]. The quantities $j_{\max}$ and $k_{\max}$ are determined by the initial chemical potential μ. Linearly increasing the orbital field with time, we trace the occupation of states in each instantaneous spectrum, defined by the time-independent Schrödinger equation $\mathcal{H}(t)|\phi_{i,k_x}(t)\rangle = E_{i,k_x}(t)|\phi_{i,k_x}(t)\rangle$. Their occupation probabilities are determined by $P_{i,k_x}(t) = \sum_{j=0}^{j_{\max}} |\langle\psi_{j,k_x}(t)|\phi_{i,k_x}(t)\rangle|^2$ [33]. At t_i, the ground state for (I), the QAH phase is determined by $\mathbf{A}(t_i) = 0$ with μ located at the Dirac point [Fig. 1(a)], whereas for (II), the QH phase, a finite background field $\mathbf{A}(t_i) = -yH_0\mathbf{e}_x$ has to be applied and μ is placed above the first LL [Fig. 1(d)]. The numerical results, presented in Figs. 1 and 2, are independent of the time scale in which $H(t)$ is ramped up, provided that $t_f^{\min} \ll t_f \ll t_f^{\max}$. The lower bound prevents excitations across bulk gaps E_g and is therefore determined by $t_f^{\min} \equiv \hbar/E_g \sim 10^{-13}$ s. For $H > H_{\mathrm{scat}}$, the upper bound comes from the requirement to overcome hybridization gaps forming between the QAH edge states and bulk LLs. As long as these hybridization

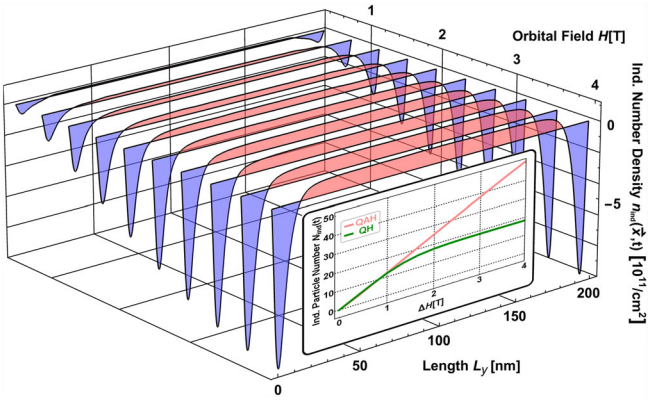

FIG. 2. Evolution of $n_{\mathrm{ind}}(\mathbf{x},t)$ in orbital fields, corresponding to Figs. 1(a)–1(c). An increase of H causes charge depletion (blue) at the edges and charge accumulation (red) in the bulk. The inset compares the induced bulk particle number $N_{\mathrm{ind}}(t) = \int d\mathbf{x} n_{\mathrm{ind}}(\mathbf{x},t)$ between the QAH (red) and the QH phase (green).

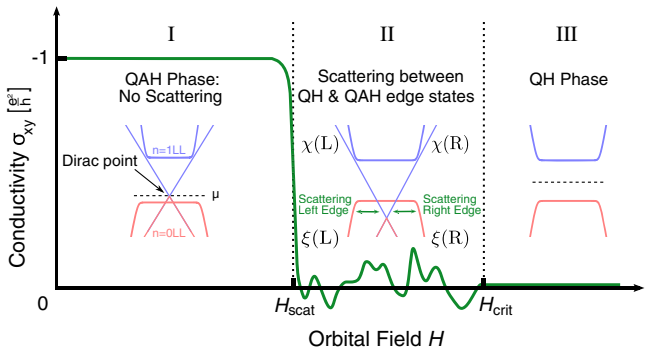

FIG. 3. Schematic evolution of σ_{xy} for a QAH insulator in orbital fields in the presence of disorder. Insets schematically illustrate the underlying band structure according to Figs. 1(a)–1(c) (same color code). In region II, scattering processes between counterpropagating QH $\xi(L/R)$ (red) and QAH $\chi(L/R)$ (blue) edge states allow for momentum and energy relaxation.

gaps are finite size gaps, exponentially suppressed by the system size, $t_f^{\max}$ tends to infinity [33].

Let us now discuss the numerical results, starting with the QAH phase under initial condition (I). Increasing $H(t)$ with time, the occupation of the eigenstates and the induced charge carrier density $j^0_{\mathrm{ind}}(\mathbf{x},t) = -en_{\mathrm{ind}}(\mathbf{x},t)$ evolve as shown in Figs. 1(a)–1(c) and Fig. 2 with $n_{\mathrm{ind}}(\mathbf{x},t) = \sum_{i,k_x} P_{i,k_x}(t)|\phi_{i,k_x}(\mathbf{x},t)|^2 - n_{\mathrm{back}}$, where n_{back} ensures that $n_{\mathrm{ind}}(\mathbf{x},t_i) = 0$. Starting from a flat (zero) charge density distribution, an increase of $H(t)$ causes a net charge flow from the QAH edge states (charge depletion) into all valence band LLs (charge accumulation). Since our system is a bulk insulator, this redistribution of charges is driven by polarization effects. As a function of the orbital field all occupied wave functions shift their spectral weight, effectively giving rise to the charge redistribution shown in Fig. 2. During this process, all valence band LLs, including the $n = 0$ LL, remain filled. As illustrated in the inset of Fig. 2, this causes a linear increase of the bulk charge with $j^0_{\mathrm{ind}} = \sigma_{xy}\nabla \times \mathbf{a} = \kappa_{\mathrm{QAH}}H(t)$. Since this type of pumping is bound to the existence of the QAH edge states, it can only exist for $H < H_{\mathrm{crit}}$ [Eq. (7)]. These results are consistent with our conclusions based on the Callan-Harvey mechanism following from Eq. (5).

In contrast, our results for the QH phase under initial condition (II) are shown in Fig. 1(d) and in the inset of Fig. 2. In agreement with our field-theoretical approach, we find that the bulk charge originates purely from the associated QH edge states, implying a saturation of the charge accumulation already for small orbital fields. This is therefore further evidence that the QAH edge states are related to a distinct CS term, which is connected to the spectral asymmetry η_H and not to a single LL.

Experimental signatures.—We have so far considered an impurity-free system. What are the consequences of taking disorder and, therefore, (in)elastic scattering into account? As long as the Dirac point is above the $n = 0$ LL, i.e., for $H < H_{\mathrm{scat}}$, the system is in its ground state. Scattering cannot cause relaxation of the induced bulk charge and, hence, disorder cannot affect the results of Figs. 1(b) and 2. The hallmark of the QAH effect is a quantized Hall plateau with $\sigma_{xy} = \kappa_{\mathrm{QAH}}$ whose length scales with $H_{\mathrm{scat}} \sim L_y^{-1}$. This is depicted by region I in Fig. 3 and follows from $g_{\mathrm{eff}} \sim L_y$ [33]. For $H > H_{\mathrm{scat}}$, the system is driven into a state with no common chemical potential, whose signature is a selective population of states (charge inversion), shown in Fig. 1(c). This charge inversion is protected by momentum conservation, since direct relaxation processes, such as spontaneous emission, are exponentially suppressed by the spatial localization of the wave functions. However, since realistic systems are rather imperfect, in(elastic) scattering between occupied QH and unoccupied QAH edge states facilitate momentum and energy relaxation as indicated by region II in Fig. 3. As a result, the charge inversion relaxes eventually, until a common chemical potential has set in. In this new ground state, counterpropagating QAH and QH edge states coexist at a single boundary. For instance in the inset of region II, at the right boundary, the QAH edge state has a positive velocity, while the QH edge state has a negative velocity. Similarly to Ref. [47], which uses the Landauer-Büttiker formalism [48,49], we expect deviations from a perfectly quantized Hall plateau arising from scattering between QH and QAH edge states. When the transmission probability $T_{i,j}$ between contacts i and j on a typical Hall bar is symmetric, meaning $T_{i,i+1} = T_{i+1,i}$, we expect a $\sigma_{xy} = 0$ plateau [33]. If scattering processes between the coexisting edge states microscopically differ on both edges of the Hall bar, deviations from a perfect quantization arise (wiggly line in Fig. 3). In contrast for $T_{i,i+1} \neq T_{i+1,i}$, the average value of σ_{xy} can significantly deviate from zero. Such direction-dependent transmission probabilities can result from a large charge puddle

density [33] (diffusive regime) which is typically present in large (Hg,Mn)Te Hall bars [50–52]. Finally, for $H > H_{\mathrm{crit}}$, the Dirac mass gap is closed and σ_{xy} vanishes as indicated by region III in Fig. 3.

Realization.—Typical materials in which this crossover should be observed include (Hg, Mn)Te/CdTe quantum wells, described by the BHZ model [20,21,25,53]. In the discussion above, we assumed that the spin-down block of the BHZ model is trivial and, hence, does not qualitatively affect the discussed physics. Nevertheless, analogous equations for the spin-down block can be derived replacing $(M, B) \to (-M, -B)$. Zeeman (g_z) and exchange (G_{ex}) terms can be incorporated, replacing $M \to M \pm g(H)$, where $g(H) \equiv g_z H \pm G_{\mathrm{ex}}(H)$ [21] and $+(-)$ applies to the spin-up(down) block. In the full BHZ model, $g \neq 0$ breaks time-reversal symmetry and drives the system into the QAH phase if $(M + g - B/l_H^2)(M - g - B/l_H^2) < 0$, extending the definition of QAH insulators to orbital fields [21]. Since the exchange interaction in (Hg,Mn)Te is paramagnetic [54], a finite orbital field is needed to drive the system into the QAH phase. In the full BHZ model, the spin-down block causes an additional transition from the QSH phase to region I in Fig. 3. In Bi-based QAH insulators, one should be able to observe similar transitions as shown in Fig. 3, given that signatures of both the QH and the QAH effect are observed at relatively small orbital fields [26–29].

Conclusions.—The field theoretical analysis of QAH insulators in orbital fields allows us to explain the very unconventional findings in band structure calculations based on the parity anomaly. In particular, we reveal three novel transport features which are all fundamentally based on the parity anomaly: a violation of the Onsager relation; a peculiar type of charge pumping with increasing orbital field; and, for large fields, the emergence of counter-propagating QH and QAH edge states. Together these signatures highlight the different physical origin of the topology of QH and QAH phases, making them distinguishable even though they are described by the same Chern number. As a fingerprint of these features, we predict a transition from $\sigma_{xy} = -e^2/h$ (QAH effect) to a noisy QH plateau with increasing orbital fields, whose average value depends on details of the QH-QAH edge state scattering. The experimental verification of our theoretical predictions in (Hg,Mn)Te quantum wells is underway [25]. In the future, it would be interesting to study signatures of quantum anomalies beyond the BHZ model and analyze microscopic signatures of counterpropagating QH and QAH edge states therein.

We thank B. Scharf, R. Meyer, B. Trauzettel, B. A. Bernevig, F. Wilczek, C. Brüne, J. S. Hofmann, J. Erdmenger, C. Morais Smith, and W. Beugeling for useful discussions. We acknowledge financial support through the Deutsche Forschungsgemeinschaft (DFG, German Research Foundation), Project-id No. 258499086—SFB 1170 "ToCoTronics," the Free State of Bavaria (Elitenetzwerk Bayern IDK "Topologische Isolatoren" and the Institute for Topological Insulators) and through the Würzburg-Dresden Cluster of Excellence on Complexity and Topology in Quantum Matter—ct.qmat (EXC 2147, Project-id No. 39085490).

*Corresponding author.
Ewelina.Hankiewicz@physik.uni-wuerzburg.de
†These authors contributed equally to this work.

[1] G. W. Semenoff, Phys. Rev. Lett. **53**, 2449 (1984).
[2] E. Fradkin, E. Dagotto, and D. Boyanovsky, Phys. Rev. Lett. **57**, 2967 (1986).
[3] F. D. M. Haldane, Phys. Rev. Lett. **61**, 2015 (1988).
[4] X. Huang, L. Zhao, Y. Long, P. Wang, D. Chen, Z. Yang, H. Liang, M. Xue, H. Weng, Z. Fang, X. Dai, and G. Chen, Phys. Rev. X **5**, 031023 (2015).
[5] Q. Li, D. E. Kharzeev, C. Zhang, Y. Huang, I. Pletikosic, A. V. Fedorov, R. D. Zhong, J. A. Schneeloch, G. D. Gu, and T. Valla, Nat. Phys. **12**, 550 (2016).
[6] C.-L. Zhang *et al.*, Nat. Commun. **7**, 10735 (2016).
[7] B. Yan and C. Felser, Annu. Rev. Condens. Matter Phys. **8**, 337 (2017).
[8] J. Gooth, A. C. Niemann, T. Meng, A. G. Grushin, K. Landsteiner, B. Gotsmann, F. Menges, M. Schmidt, C. Shekhar, V. Süß, R. Hühne, B. Rellinghaus, C. Felser, B. Yan, and K. Nielsch, Nature (London) **547**, 324 (2017).
[9] K. Fujikawa, Phys. Rev. D **21**, 2848 (1980).
[10] R. A. Bertlmann, *Anomalies in Quantum Field Theory* (Oxford University Press, New York, 1996).
[11] M. Nakahara, *Geometry, Topology and Physics*, edited by T. Spicer (Institute of Physics Publishing, Bristol and Philadelphia, 2003).
[12] A. J. Niemi and G. W. Semenoff, Phys. Rev. Lett. **51**, 2077 (1983).
[13] A. J. Niemi and G. W. Semenoff, Phys. Rev. D **30**, 809 (1984).
[14] R. Jackiw, Phys. Rev. D **29**, 2375 (1984).
[15] A. J. Niemi, Nucl. Phys. **B251**, 155 (1985).
[16] A. N. Redlich, Phys. Rev. D **29**, 2366 (1984).
[17] D. Boyanovsky, R. Blankenbecler, and R. Yahalom, Nucl. Phys. **B270**, 483 (1986).
[18] A. M. J. Schakel, Phys. Rev. D **43**, 1428 (1991).
[19] M. Mulligan and F. J. Burnell, Phys. Rev. B **88**, 085104 (2013).
[20] B. A. Bernevig, T. L. Hughes, and S.-C. Zhang, Science **314**, 1757 (2006).
[21] C. X. Liu, X.-L. Qi, X. Dai, Z. Fang, and S.-C. Zhang, Phys. Rev. Lett. **101**, 146802 (2008).
[22] A. P. Schnyder, S. Ryu, A. Furusaki, and A. W. W. Ludwig, Phys. Rev. B **78**, 195125 (2008).
[23] We take the spin-up block of the BHZ model with a nontrivial Chern number $\mathcal{C} = -1$ at $H = 0$.
[24] H.-Z. Lu, W.-Y. Shan, W. Yao, Q. Niu, and S.-Q. Shen, Phys. Rev. B **81**, 115407 (2010).

[25] A. Budewitz, S. Shamim, K. Bendias, P. Leubner, T. Khouri, S. Wiedmann, H. Buhmann, and L. W. Molenkamp (to be published).
[26] C.-Z. Chang *et al.*, Science **340**, 167 (2013).
[27] J. G. Checkelsky, R. Yoshimi, A. Tsukazaki, K. S. Takahashi, Y. Kozuka, J. Falson, M. Kawasaki, and Y. Tokura, Nat. Phys. **10**, 731 (2014).
[28] C.-Z. Chang, W. Zhao, D. Y. Kim, P. Wei, J. K. Jain, C. Liu, M. H. W. Chan, and J. S. Moodera, Phys. Rev. Lett. **115**, 057206 (2015).
[29] A. J. Bestwick, E. J. Fox, X. Kou, L. Pan, K. L. Wang, and D. Goldhaber-Gordon, Phys. Rev. Lett. **114**, 187201 (2015).
[30] B. Scharf, A. Matos-Abiague, and J. Fabian, Phys. Rev. B **86**, 075418 (2012).
[31] B. Zhou, H.-Z. Lu, R.-L. Chu, S.-Q. Shen, and Q. Niu, Phys. Rev. Lett. **101**, 246807 (2008).
[32] M. König, H. Buhmann, L. W. Molenkamp, T. L. Hughes, C.-X. Liu, X.-L. Qi, and S.-C. Zhang, J. Phys. Soc. Jpn. **77**, 031007 (2008).
[33] See Supplemental Material at http://link.aps.org/supplemental/10.1103/PhysRevLett.123.226602 for further details on Chern insulators in orbital fields, the effective action, the parity symmetry. the numerical method, and transport signatures of counterpropagating QH and QAH edge states.
[34] S. Deser, R. Jackiw, and S. Templeton, Ann. Phys. (N.Y.) **140**, 372 (1982).
[35] J. Böttcher, C. Tutschku, and E. M. Hankiewicz (to be published).
[36] X. G. Wen, Phys. Rev. B **43**, 11025 (1991).
[37] S. Chandrasekharan, Phys. Rev. D **49**, 1980 (1994).
[38] C. G. Callan and J. A. Harvey, Nucl. Phys. **B250**, 427 (1985).
[39] R. Nakai, S. Ryu, and K. Nomura, Phys. Rev. B **95**, 165405 (2017).
[40] E. Fradkin, *Field Theories of Condensed Matter Physics*, edited by S. Capelin (Cambridge University Press, Cambridge England, 2013).
[41] M. Stone and F. Gaitan, Ann. Phys. (N.Y.) **178**, 89 (1987).
[42] N. Maeda, Phys. Lett. B **376**, 142 (1996).
[43] E. G. Novik, A. Pfeuffer-Jeschke, T. Jungwirth, V. Latussek, C. R. Becker, G. Landwehr, H. Buhmann, and L. W. Molenkamp, Phys. Rev. B **72**, 035321 (2005).
[44] C. Brüne, C. X. Liu, E. G. Novik, E. M. Hankiewicz, H. Buhmann, Y. L. Chen, X. L. Qi, Z. X. Shen, S. C. Zhang, and L. W. Molenkamp, Phys. Rev. Lett. **106**, 126803 (2011).
[45] Y. Baum, J. Böttcher, C. Brüne, C. Thienel, L. W. Molenkamp, A. Stern, and E. M. Hankiewicz, Phys. Rev. B **89**, 245136 (2014).
[46] A. Messiah, *Quantum Mechanics* Vol. 2, North-Holland Series in Physics (North-Holland, Amsterdam, 1965).
[47] J. Wang, B. Lian, H. Zhang, and S.-C. Zhang, Phys. Rev. Lett. **111**, 086803 (2013).
[48] M. Büttiker, Phys. Rev. B **33**, 3020 (1986).
[49] M. Büttiker, Phys. Rev. B **38**, 9375 (1988).
[50] J. I. Väyrynen, M. Goldstein, and L. I. Glazman, Phys. Rev. Lett. **110**, 216402 (2013).
[51] L. Lunczer, P. Leubner, M. Endres, V. L. Müller, C. Brüne, H. Buhmann, and L. W. Molenkamp, Phys. Rev. Lett. **123**, 047701 (2019).
[52] A. Roth, C. Brüne, H. Buhmann, L. W. Molenkamp, J. Maciejko, X.-L. Qi, and S.-C. Zhang, Science **325**, 294 (2009).
[53] D. G. Rothe, R. W. Reinthaler, C. X. Liu, L. W. Molenkamp, S.-C. Zhang, and E. M. Hankiewicz, New J. Phys. **12**, 065012 (2010).
[54] J. K. Furdyna, J. Appl. Phys. **64**, R29 (1988).